Astron. Astrophys. 334, 269–279 (1998)

ASTRONOMY AND ASTROPHYSICS

# Cores and cavities in NGC 1333

**B. Lefloch**[1,2], **A. Castets**[2], **J. Cernicharo**[1], **W.D. Langer**[3], **and R. Zylka**[4]

[1] Consejo Superior de Investigaciones Científicas, Instituto de Estructura de la Materia, Departamento Física Molecular, Serrano 123, E-28006 Madrid, Spain
[2] Laboratoire d'Astrophysique, Observatoire de Grenoble, BP 53X, F-38041 Grenoble Cedex 9, France
[3] Jet Propulsion Laboratory, California Institute of Technology, Pasadena, CA 91109, USA
[4] Institut fuï Theoretische Astrophysik (ITA), Universtität Heidelberg, Tiergartenstr. 15, D-69121 Heidelberg, Germany

Received 22 September 1997 / Accepted 10 February 1998

**Abstract.** We present 1.3mm continuum and CS $J = 5 \rightarrow 4$ maps at $12''$ resolution of the NGC1333 star forming region. The area covered is $8' \times 6'$. The large-scale bolometer and CS maps delineate very nicely the large central cavity together with the cores situated in the surrounding compressed shell. In addition to the four dust cores IRAS4A-B, IRAS2 and SVS13, we discovered two fainter condensations, one of which is not associated with protostellar activity. All protostars are surrounded by extended low-emissivity envelopes and show indications of depletion of molecules onto grains. The continuum emission traces material entrained by the outflows powered by IRAS4A, IRAS2 and SVS13. The CS $J = 5 \rightarrow 4$ is observed in all dust cores. Apart from IRAS4, the CS emission peak is shifted with respect to the dust continuum. The large-scale dust emission mostly comes from material compressed around two cavities, whose walls are detected in the $H_2$ S(1) v= 1-0 line. These cavities seem to have been excavated by outflows from the neighboring protostars IRAS4 and SVS13, and are now expanding in the ambient medium. Taken together these new data suggest that the large cavity in NGC1333 grows by local action of stars forming in the compressed edge, each producing a local cavity which eventually overlap.

**Key words:** ISM: individual objects: NGC 1333 – ISM: jets and outflows – ISM: molecules – radio continuum: ISM – radio lines: ISM – stars: formation

## 1. Introduction

NGC1333 is a long studied example of recent and active star forming region. It is located at an estimated distance of $350$ pc (Cernicharo et al. 1985). Infrared observations have revealed a cluster of about 150 low and intermediate mass stars (Aspin et al. 1994; Aspin et al. 1997; Lada et al. 1997). Many far-infrared young stellar objects and Class 0 sources have been discovered in the molecular gas (Jennings et al. 1987; Sandell et al. 1991, 1994). Evidences of interaction between the protostars and the circumstellar environment like $H_2$ jets, Herbig-Haro objects and molecular outflows have been widely reported. Altogether, these observations draw the picture of a large-scale star forming burst occurring in NGC1333. Warin et al. (1996, hereafter WCLWP) and Langer et al. (1996, hereafter LCL) reported the presence of a large pear-shaped cavity in the center of the cloud and suggested it was created by the outflows arising from these sources. These outflows might also be responsible for the compression of the surrounding shell and the initiation of the next generation of young stellar objects.

Among all protostars discovered in this region, only IRAS4 and SVS13 have been studied in the millimeter and submillimeter continuum (Sandell et al. 1990, 1991; Lay et al. 1995). Numerous molecular studies have been devoted to SVS13, IRAS4 and IRAS2 (Bachiller & Cernicharo 1990; Sandell et al. 1994; Blake et al. 1995; WCLWP; Mehringer 1996; LCL; Ward-Thompson et al. 1996). However there is no systematic study at high resolution of the whole region in the continuum emission nor any molecular high density tracers, such as CS $J = 5 \rightarrow 4$ . To strengthen our picture of star formation in NGC1333, we have undertaken a large scale mapping at high angular resolution of this region in the CS millimeter lines and dust continuum using the IRAM 30m telescope (Pico Veleta, Spain). In this paper we compare the millimeter continuum emission, tracing the dust column density, and some CS $J = 5 \rightarrow 4$ observations, tracing high-density gas, together with a published $H_2$ map of this region to study how the various sources have interacted with the molecular gas to create the cavities and shape the surrounding gas.

## 2. Observations

### *2.1. Continuum observations*

The observations were carried out in March 1995 and 1996 with the MPIfR 19-channel bolometer array, operating at 1.25mm, installed at the IRAM 30m-telescope. The resolution of the telescope is $11''$. The final map was obtained by combining several individual fields, centered on the brightest sources of NGC1333. Each field was scanned in the Azimuth direction by moving the telescope at a speed of $4''$ per sec; subsequent azimuth scans

*Send offprint requests to*: Bertrand.Lefloch@obs.ujf-grenoble.fr

were displaced by 4″ (≈ one-third of a telescope beam). We used a chopping secondary at 2 Hz with a throw of 45″. Calibration was checked against Uranus and Mars and skydips were performed regularly. The weather conditions were rather stable during the observing sessions.

### *2.2. Molecular observations*

In September 1995 we observed with the IRAM 30m telescope the $J = 2 \rightarrow 1$, $J = 3 \rightarrow 2$ and $J = 5 \rightarrow 4$ transitions of the CS molecule. Details about the observing procedure are given in LCL. The data were taken with a sampling of 12″. We used an autocorrelator as spectrometer, which provided a velocity resolution of $\approx 0.1$ km s$^{-1}$. Additional $C^{18}O$ $J = 1 \rightarrow 0$ and $J = 2 \rightarrow 1$ observations were done in December 1996 and July 1997 at selected points in and around the dust condensations.

## 3. Dust emission

Fig. 1 shows the continuum emission of the entire region mapped. The resolution of this map has been degraded to 15″ (0.03 pc) in order to detect the presence of weak extended emission. The rms is 6 mJy per 15″ beam, which enables us to detect condensations with masses higher than $0.03$ M$_\odot$ in one beam at the $3\sigma$ confidence level (see Sect. 3.4 for mass determinations from the continuum flux). However, all the millimeter fluxes quoted in this work are extracted from the original - undegraded - map, whose resolution is 11″ (0.02 pc). All sizes quoted in this article refer to sizes deconvolved from the telescope lobe (11″).

The North-West region in Fig. 1 is devoid of any continuum emission. It coincides with the large cavity reported and discussed by WCLWP and LCL. The cavity is neatly delineated and surrounded by a weak extended component which coincides with the CS emission (see LCL). Around the large cavity, and in addition to the three protostellar cores IRAS2, SVS13 and IRAS4, we find two other dust condensations. The brightest of them appears as a condensation with a peak flux of $\approx 255$ mJy beam$^{-1}$ embedded in an extended envelope of low-emissivity. Peaking at offset (100″, 140″), it is associated with IRAS7 and two other near-infrared sources reported by Aspin et al. (1994). The core is approximately elliptical with a projected angle (P.A.) of 20°. It has a major and minor axis of $0.058$ pc and $0.026$ pc respectively. Our recent CS millimeter molecular observations reported in LCL show that, in addition to the HH6 object, this continuum source drives a CS outflow.

The other condensation is much fainter; it is located on the border of the cavity at offsets (50″,80″). Its peak flux is 57 mJy beam$^{-1}$ and it does not contain any IR source or evidence of outflow motions.

### *3.1. IRAS2*

The source IRAS2 was identified from IRAS PSC observations by Jennings et al. (1987) and found to have only weak emission at 12 and 25 $\mu$m. It is associated with two bipolar outflows (Liseau et al. 1988) of very different kinematical ages. Sandell et al. (1994) found strong submillimeter emission from IRAS2, in a $\sim 20''$ beam, and suggested that it might actually be a binary system. Our observations show that IRAS2 consists of a bright source with a peak flux of 310 mJy beam$^{-1}$ surrounded by a low-emissivity envelope traced by the $50$ mJy beam$^{-1}$ contour (Fig. 2). This level defines an elliptical core of 0.13 by 0.066 pc. The major axis of this core makes a P.A. of $-60°$. Some more collimated emission seems to be superimposed upon the overall elliptical dust distribution, notably in the Eastern part of the core. The size of the central source is 12″, i.e. barely resolved by the telescope beam (11″). This is 1.5 times as large as the size *assumed* by Sandell et al. (8″) although still compatible with their assumption. The brightness distribution inside the IRAS2 central core does not show any flattening down to a 6″ scale (half-beam); so that down to 2100 AU, we do not find any evidence for a binary protostellar system, in agreement with Hodapp & Ladd (1995, hereafter HL95). Molecular millimeter observations including high-density gas tracers reveal no strong peak at the position of the IRAS2 source (this paper and Sandell et al. 1994). This indicates depletion or optically thick emission.

### *3.2. IRAS4*

IRAS4, early recognized as a Class 0 source, is one of the best studied protostellar objects (Jennings et al. 1987; Sandell et al. 1991; Blake et al. 1995; Lay et al. 1995). Sandell et al. (1991) were the first to show that IRAS4 actually consists of two bright protostellar objects IRAS4A and 4B. Recent interferometric continuum observations by Lay et al. (1995) have revealed that IRAS4A and 4B are themselves multiple protostar systems. The double system (IRAS4A and B) lies inside a well delineated clump (60″ × 40″), oriented SE-NW (see Fig. 3). To the Southeast of IRAS4B, the clump has an elongated low-emissivity tail, $\approx 45''$ wide, which we could detect over $70''$ up to the border of Fig. 1, beyond which the tail seems to continue.

IRAS4A peaks at position $(90'', -150'')$ with a peak flux of $\simeq 3.10$ Jy beam$^{-1}$ (see Fig. 3). The IRAS4A emission arises from a circular condensation of diameter $0.016$ pc (9.4″), with two long and relatively bright (the flux density is $\geq 0.25$ Jy beam$^{-1}$) extensions oriented North-South $\approx 0.02$ pc ($10'' - 15''$). These extensions have the same orientation as the CS $J = 7 \rightarrow 6$ outflow observed by Blake et al. (1995) (see Fig. 3). In addition, the southern extension spatially coincides with the $H_2$ S(1) nebulosity detected by HL95 (see feature 6 in their Fig. 1). IRAS4B is connected to IRAS4A by a bridge of lower continuum emission and peaks 30″ to the south east with a peak flux of $\simeq 1.25$ Jy beam$^{-1}$. The IRAS4B dust distribution traces an elliptical core of 0.024 by 0.014 pc, which has a small southern extension, associated with the CS $J = 7 \rightarrow 6$ red wing and the $H_2$ knots observed by Blake et al. (1995) and Hodapp & Ladd (1995) (marked 9 in their Fig. 1 and Fig. 3 in this paper).

### *3.3. SVS13*

SVS13 is a bright infra-red Class I source (Strom et al. 1976; Jennings et al. 1987) which drives the HH7–11 objects and a

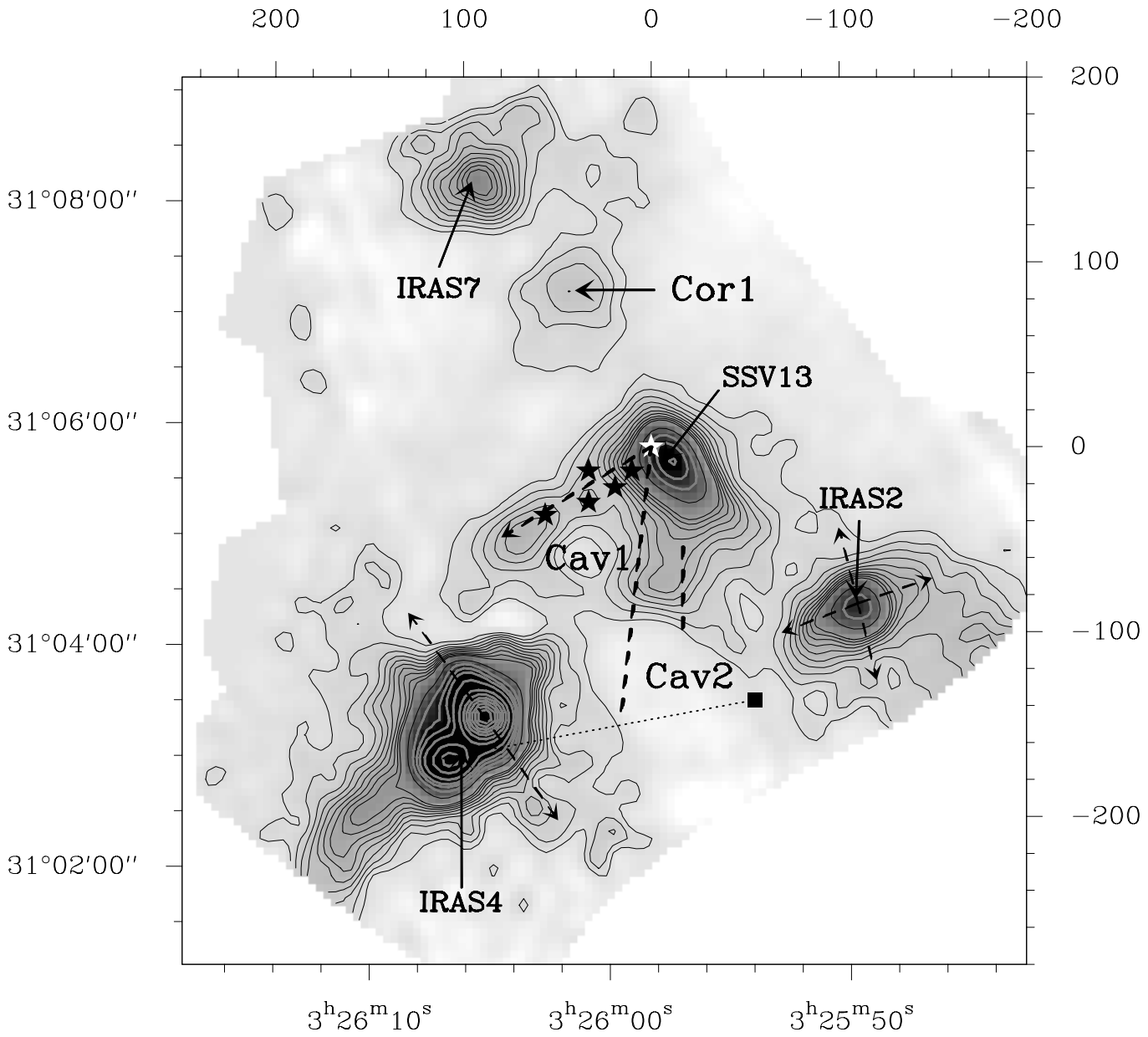


**Fig. 1.** Continuum emission at 1.25mm of the NGC1333 star forming region obtained with the IRAM 30m radiotelescope. The resolution of this map is $15''$. The (0,0) position indicated by the star corresponds to the location of SVS13, at $\alpha$(1950) = $03^h25^m58.3^s$ and $\delta$(1950) = $31°05'49''$. The upper and right hand scales are offsets in arcseconds. Contour levels range from 10 to 100 mJy beam$^{-1}$ by 10 mJy beam$^{-1}$, 150 to 300 mJy beam$^{-1}$ by 50 mJy beam$^{-1}$, 0.40 to 3.00 Jy beam$^{-1}$ by 0.20 Jy beam$^{-1}$. Cor1, Cav1, Cav2 indicate the positions of the core and cavities described in the text. Herbig-Haro objects 7 to 11 are marked by black stars. The molecular outflows and the $H_2$ filaments discussed in the text are indicated by dashed lines. The dotted line traces the direction of the jet which could be responsible for digging cavity Cav2, the bow-shock of which is marked by a black square.

high-velocity CO outflow (Bachiller & Cernicharo 1990). Interferometric observations at 3 mm have revealed the presence of a companion $15''$ to the south-west (Grossman et al. 1987). In agreement with millimeter and submillimeter observations at lower spatial resolution ($20''$) and sensitivity performed by Sandell et al. (1990), we find that the continuum emission defines an elliptic core of 0.066 by 0.029 pc ($38.5''$ by $17''$) oriented perpendicularly to the HH 7-11 outflow and slightly offset from SVS13 (see Fig. 4). The peak flux (0.32 Jy beam$^{-1}$) is located between SVS13 and its companion. The core is well delineated by the contour at 80 mJy beam$^{-1}$. At the eastern edge of the core protrudes a weak emission lane oriented South-East (35 - 55 mJy beam$^{-1}$) which overlaps with the HH 7-11 high-velocity molecular outflow and the associated $H_2$ jet. The spatial coincidence between the maxima of dust emission and the jet suggests that part of the millimeter flux originates from the outflowing

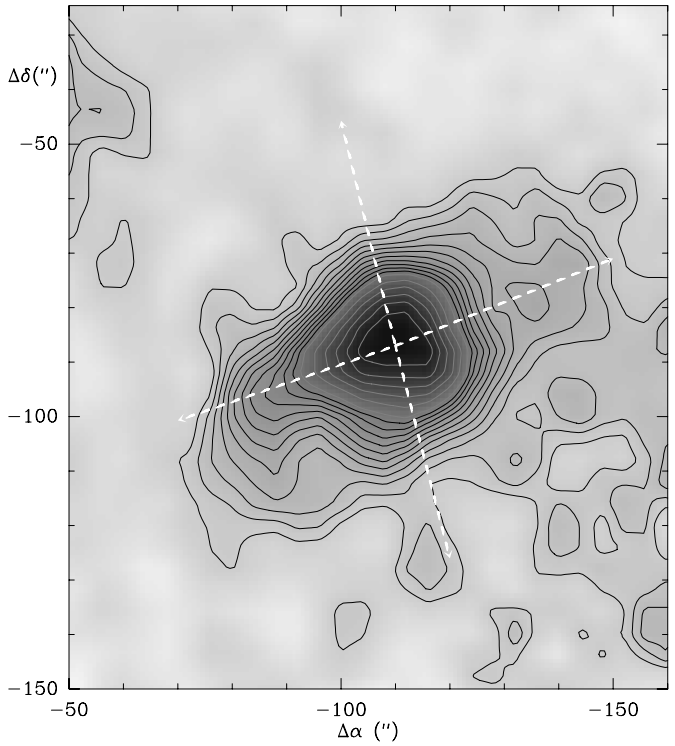


**Fig. 2.** Contour map of the 1.25mm continuum emission from NGC1333/IRAS2. Axes offsets are in arcseconds from SVS13. The resolution of this map is $11''$. The peak flus is $310$ mJy $\mathrm{beam}^{-1}$. Contours range from $30$ mJy beam$^{-1}$ ($3\sigma$) to $140$ mJy $\mathrm{beam}^{-1}$ by steps of $10$ mJy beam$^{-1}$, then from 160 to 310 mJy $\mathrm{beam}^{-1}$ by steps of $20$ mJy $\mathrm{beam}^{-1}$. The dashed lines trace the directions of the molecular outflows associated with the IRAS2 molecular core. The younger and more powerful outflow is oriented $\approx$ East-West, along the main axis of the IRAS2 envelope.

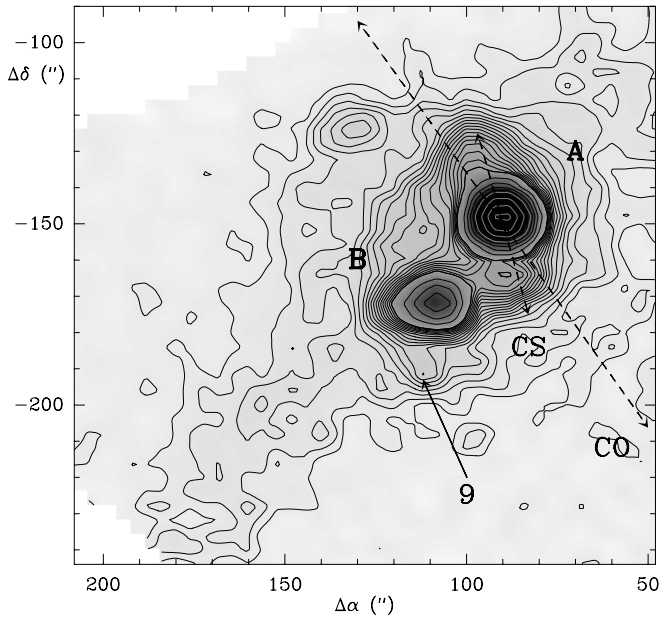


**Fig. 3.** Contour map of the 1.25mm continuum emission from NGC1333/IRAS4. Axes offsets are in arcseconds from SVS13. The resolution of the map is $11''$. The lowest contour is 30 mJy beam$^{-1}$ ($3\sigma$). Contours go from 30 to 540 mJy beam$^{-1}$ by steps of 30 mJy beam$^{-1}$, then from 0.54 to 1.34 Jy beam$^{-1}$ by 200 mJy beam$^{-1}$ and from 1.50 Jy beam$^{-1}$ to the maximum by 0.50 Jy beam$^{-1}$. IRAS4A and IRAS4B peak fluxes are 3.10 Jy beam$^{-1}$ and 1.25 Jy beam$^{-1}$ respectively. The dashed lines trace the directions large-scale CO outflow and the small-scale CS(7-6) outflow. Mark 9 indicates the position of the $H_2$ knot and the red CS(7-6) wing associated with IRAS4B (see Sect. 3.2).

gas itself. However, the continuum emission extends beyond the $H_2$ emission, i.e. it reveals material distinct from that entrained by the flow. To the south the core emission is prolonged by an extension over $30''$ in length, barely apparent in the observations of Sandell et al. (1990). It lies actually between the western limb of the $H_2$ "V-feature" to the East and the ASR 20-21 filament to the West, as can be seen on Fig. 4 (see also Fig. 1 of HL95).

### *3.4. Core masses*

To convert continuum fluxes into masses, we adopted the standard dust model by Draine & Lee (1984), which makes use of an opacity law $\kappa_\nu = \kappa_0\,(\lambda/\lambda_0)^{-2}$ with $\kappa_0 = 0.05$ cm$^2$g$^{-1}$ at $\lambda_0 = 250\mu m$. In order to account for variations of the dust absorption cross-section due to molecule freezing onto grains around deeply embedded sources, we followed the same approximation as in Mezger et al. (1990), i.e. we took $\kappa_0 = 0.09$ cm$^2$g$^{-1}$ in the core of the Class 0 sources IRAS2, IRAS4A and IRAS4B. In the calculations the dust temperature was chosen to be 20 K in IRAS2, 33 K in IRAS4 and 40 K in SVS13, IRAS7 and Cor1.

In IRAS2 Sandell et al. (1994) determined from submillimeter continuum observations a dust temperature of 26 K, while Ward-Thomson et al. (1997) estimated from their infall model that the kinetic temperature of the IRAS2 envelope lies in the range 15-20 K. Therefore, for this very embedded source, the adopted value of 20 K seems realistic. The 33K IRAS4 temperature is derived from fitting the spectral energy distribution obtained by Sandell et al. (1991) from submillimeter photometry. This value is also equal to the IRAS color temperature quotted by Jennings et al.(1987). In SVS13 we adopted the dust temperature obtained from high spatial resolution ($10''$) continuum measurements by Grossman et al. (1987), a value also in agreement with the IRAS color temperature of Jennings et al. (1987). This temperature agrees also very well with the temperature obtained from the excitation conditions of $HCO^+$ in this region (Dent et al. 1993). Finally because IRAS7 and Cor1 are situated in a region of lower density with numerous infrared sources (LCL), we have assumed the same dust temperature as in the nearby SVS13 core, i.e. $T_d = 40$K. We also adopted $D_{kpc}$ = 0.35.

IRAS2 appears in the continuum emission to be composed of a spherical core surrounded by a lower intensity elliptical feature. For this source, we estimate a mass of $0.8$ M$_\odot$ out to a radius of $6''$. If we take into account the lower-density envelope, we obtain $4.2$ M$_\odot$ for the total mass of the IRAS2 core. This implies a mean $H_2$ density $n(H_2) = 2.4\,10^5$ cm$^{-3}$ throughout

**Table 1.** Physical parameters of the dust cores in NGC1333 : Flux, Size and Mass of the dust condensations. The peak flux ($S_{1.25\ mm}$) is given in the fourth column. At the exception of IRAS2, the integrated fluxes ($S^{int}_{1.25\ mm}$), sizes, total masses and mean densities are given for the whole condensation (central source + envelope). In the second and third column are mentioned the values adopted for the opacity $\kappa_0$ and the dust temperature $T_d$. K is the ratio of the estimates of $H_2$ column density derived from $C^{18}O$ and dust respectively.

| Name | $\kappa_0$ $cm^2g^{-1}$ | $T_d$ K | $S_{1.25\ mm}$ Jy beam$^{-1}$ | $S^{int}_{1.25\ mm}$ Jy | Size ($''\times''$) | Mass $M_\odot$ | n($H_2$)$^a$ $cm^{-3}$ | n($H_2$)$^b$ $cm^{-3}$ | N($H_2$)$^c$ $10^{23}$ cm$^{-2}$ | N($H_2$)$^d$ $10^{23}$ cm$^{-2}$ | K |
|---|---|---|---|---|---|---|---|---|---|---|---|
| SVS13 | 0.05 | 40 | 0.32 | 1.9 | $39\times17$ | 3.5 | $2.1\,10^6$ | $5.0\,10^5$ | 1.0 | 0.34 | 0.34 |
| IRAS2 (core) | 0.09 | 20 | 0.31 | 0.38 | 12 | 0.8 | $3.0\,10^6$ | $3.0\,10^6$ | 1.8 | 0.17 | 0.096 |
| (envelope) | 0.05 | 20 | - | 1.1 | $76\times39$ | 4.2 | $2.4\,10^5$ | $\sim 2\,10^5$ | 0.50 | 0.14 | 0.2-0.4 |
| IRAS4A | 0.09 | 33 | 3.1 | 4.7 | 9.4 | 6.2 | $4.9\,10^7$ | $2.0\,10^6$ | 3.7 | 0.21 | 0.057 |
| IRAS4B | 0.09 | 33 | 1.3 | 1.6 | $21.4\times9.6$ | 2.1 | $7.0\,10^6$ | $4.0\,10^5$ | 2.1 | 0.20 | 0.093 |
| IRAS7 | 0.05 | 40 | 0.25 | 0.54 | $55\times34$ | 1.3 | $1.3\,10^5$ | $4.6\,10^5$ | 0.25 | 0.35 | 1.4 |
| Cor1 | 0.05 | 40 | 0.057 | 0.25 | $\sim 38$ | 0.46 | $5.5\,10^4$ | $3.3\,10^5$ | 0.12 | 0.30 | 2.5 |

[a] estimated from dust continuum observations.
[b] estimated from CS observations (LCL).
[c] estimated from dust continuum observations.
[d] estimated from $C^{18}O$ $J=1\rightarrow0$ observations, assuming an abundance factor $[H_2]/[C^{18}O] = 4\,10^6$ (Cernicharo & Guélin 1987).

the central source together with an associated visual extinction $A_v \sim 160$ mag. However the elliptical halo could be the result of heating due to the interaction of the outflow and the ambient material and its temperature could be higher than in the IRAS2 core.

The extended emission surrounding IRAS4A and 4B makes their mass determination rather uncertain. We have defined the sizes of the components by the lowest brightness contour which isolates both condensations (500 mJy beam$^{-1}$). Assuming a dust temperature of 33K (see above), we obtain masses of 6.2 and 2.1 $M_\odot$ for IRAS4A and 4B, respectively (including emission of the parental cocoon above 500 mJy). These results are in good agreement with values obtained by Sandell et al. (1991) and Blake et al. (1994).

We find that the core of SVS13 is well delineated by the contour at 80 mJy beam$^{-1}$. Hence adopting a dust temperature of 40 K, we obtain for SVS13 a total mass of 3.5 $M_\odot$. Sandell et al. (1990) obtained $13\,M_\odot$ in the same region, because of a larger integrated flux (their beam is $\approx$ twice as large as the beam of the 30m telescope), and a lower dust temperature (they adopted $T_d = 20\,K$). While the dust temperature is still an open question, we feel confident in our total flux value because our observations were made with higher resolution and sensitivity. Finally, for the IRAS7 and Cor1 cores to the north of SVS13 we estimate their masses as 1.3 $M_\odot$ and 0.46 $M_\odot$ respectively.

From the protostellar masses derived and the size of the whole condensations, we estimate mean core densities ranging from $5\,10^4$ cm$^{-3}$ for Cor1 to $5\,10^7$ cm$^{-3}$ for IRAS4A, i.e. comparable to or larger than the CS critical density. The highest densities were obtained for the youngest protostars, at the exception of IRAS2. This is due to the large extent of its envelope (larger than for the other sources); if one concentrates on the central condensation, we obtain typical densities of $3\,10^6$ cm$^{-3}$, comparable to the densities of the other protostellar cores.

### *3.5. High-velocity outflows*

Our millimeter continuum observations show strong evidence for a correlation between continuum emission and the entrained material of molecular outflows or HH objects (see Fig. 1), around all the protostellar sources detected and especially around the most embedded objects. The contribution of the gas to this emission is however difficult to estimate.

The case of IRAS2 is all the more remarkable as the flow could be traced back to the protostellar source only in the millimeter SiO lines and only in one lobe (Lefloch et al. 1997). On the contrary, the material entrained is revealed clearly in the bolometer map and causes the elongated shape of the IRAS2 core observed *in the direction* of the outflow (see Fig. 2 and Fig. 1). Similarly, we observe in IRAS4A two long and bright continuum extensions (Fig. 1 and Fig. 3) which connect with the outflow lobes as traced by the CS and SiO lines (Blake et al 1995; Lefloch et al. 1997).

### *3.6. Dust cavities*

Our continuum map shows a "hole" in the continuum emission between SVS13 and IRAS4, centered at offset $(40'', -65'')$, that we refer to as Cav1 in what follows (see Fig. 1 and Fig. 4). This cavity is bounded to the North by the bridge of gas and dust overlapping with the HH 7-11 outflow and to the West by the southern extension protruding from the SVS13 core. South of Cav1 appears another cavity centered at offset $(+25'', -125'')$ (Cav2 in Fig. 1 and Fig. 4)). In the following section, we discuss the kinematics of the dense gas (as traced by the CS $J=5\rightarrow4$ line) around the dust cavities and the protostellar sources.

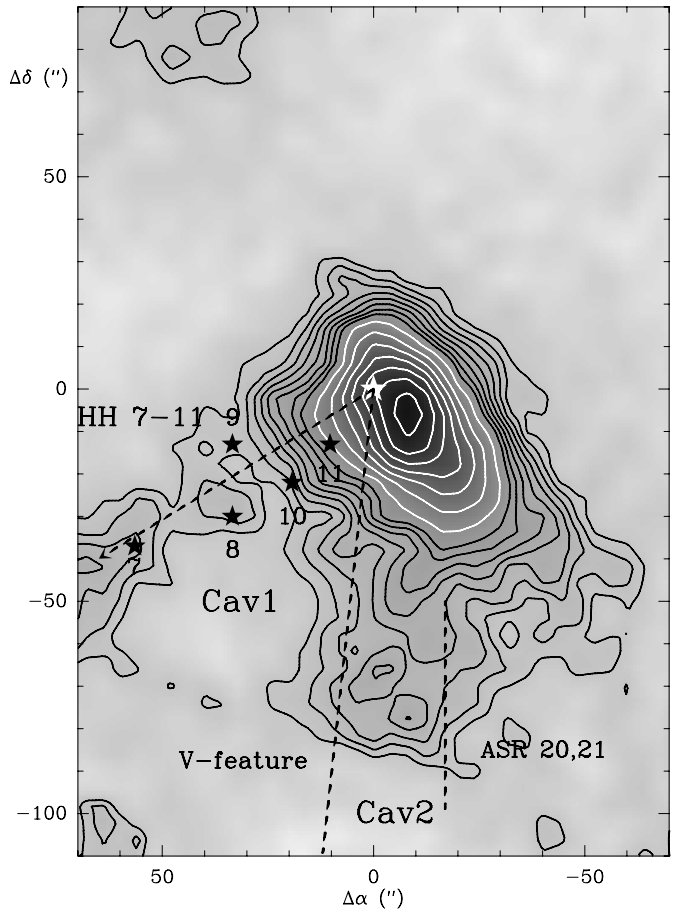


**Fig. 4.** Contour map of the 1.25 mm continuum emission from NGC1333/SVS13. Axes offsets are in arcseconds. The resolution of the map is $11''$. Contours go from 30 mJy beam$^{-1}$ ($3\sigma$) to 100 mJy beam$^{-1}$ by 10 mJy beam$^{-1}$, and from 120 mJy beam$^{-1}$ to the maximum by 30 mJy beam$^{-1}$. The SVS13 peak flux is 0.32 Jy beam$^{-1}$. The dashed lines indicate the molecular outflow and jet HH 7-11, and two $H_2$ filaments, one of which traces the wall of Cav1. Positions of the Herbig-Haro objects HH 7 to 11 are marked by black stars.

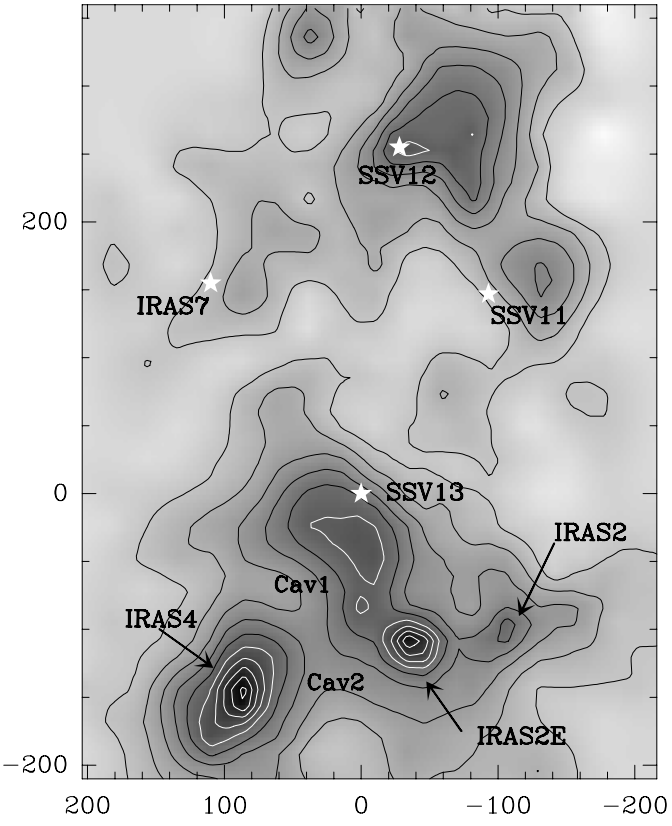


**Fig. 5.** Contour map of the CS $J = 5 \rightarrow 4$ emission integrated over velocities from 6 to 9 km s$^{-1}$. First contour and contour interval are 3 K km s$^{-1}$. The (0, 0) position indicated by a star correspond to the location of SVS 13. Cav1 and Cav2 indicate the position of the two cavities discussed in the text (Sect. 2.5 and 3.3).

## 4. Molecular emission

### *4.1. CS maps*

The results of the CS $J = 3 \rightarrow 2$ and $J = 2 \rightarrow 1$ observations were presented in LCL. Both maps are very similar. They show that the central cavity of NGC1333 is surrounded by a dense compressed shell at 8 km s$^{-1}$ and a second gas layer at 7 km s$^{-1}$ located inside the cavity. The CS $J = 5 \rightarrow 4$ observations, which trace the very dense and perhaps hotter gas, look slightly different. Most of the $J = 5 \rightarrow 4$ emission is comprised between 6 and 9 km s$^{-1}$; outside this velocity range, emission arises from shocked gas centered on IRAS4 and the East bow-shock of IRAS2 (IRAS2E). Fig. 5 shows the CS $J = 5 \rightarrow 4$ emission integrated over velocities from 6 to 9 km s$^{-1}$. In the northern part of the map, we see two CS cores which correspond to SVS11 and SVS12. The high-density gas which connects these two cores contain several near-infrared sources identified by Aspin et al. (1994) and Lada et al. (1996). Also, the large cavity identified by WCLWP and LCL which appears pear-shaped in the $J = 3 \rightarrow 2$ line, is open to the East and to the West in the $J = 5 \rightarrow 4$ emission.

At velocities $< 7.2$ km s$^{-1}$, there is an *apparent* connection between IRAS4, the East bow-shock of IRAS2 (IRAS2E) and a condensation south of SVS13 (see e.g. planes **a** and **b** in Fig. 6). This connection is barely seen in CS $J = 3 \rightarrow 2$ . Below this bridge appears a hole in the CS emission, bounded to the south (Fig. 6a). This hole is detected at blueshifted velocities and also in the layer at $v = 7.2$ km s$^{-1}$. It therefore traces a cavity surrounded by dense gas blueshifted by $\approx 0.5 - 1$ km s$^{-1}$. We have not found any counterpart at redshifted velocities ($v \geq 8.5$ km s$^{-1}$). Due to its spatial coincidence with Cav2, it is probably the molecular counterpart of this cavity (see Fig. 7a). Similarly, we unambiguously detect a cavity in the CS emission at the position of Cav1 which suggests that both are associated (see Fig. 7b). This cavity shows up only in the redshifted gas ($v \geq 8.2$ km s$^{-1}$).

The dynamics of the gas close to SVS13 is intriguing. We detect a CS core south of the SVS13 continuum peak (cf. Fig. 5 and 6d). This condensation appears displaced with respect to the SVS13 dust core. We note however that higher angular resolution observations (Rudolph et al. 1997) show that SVS13 is

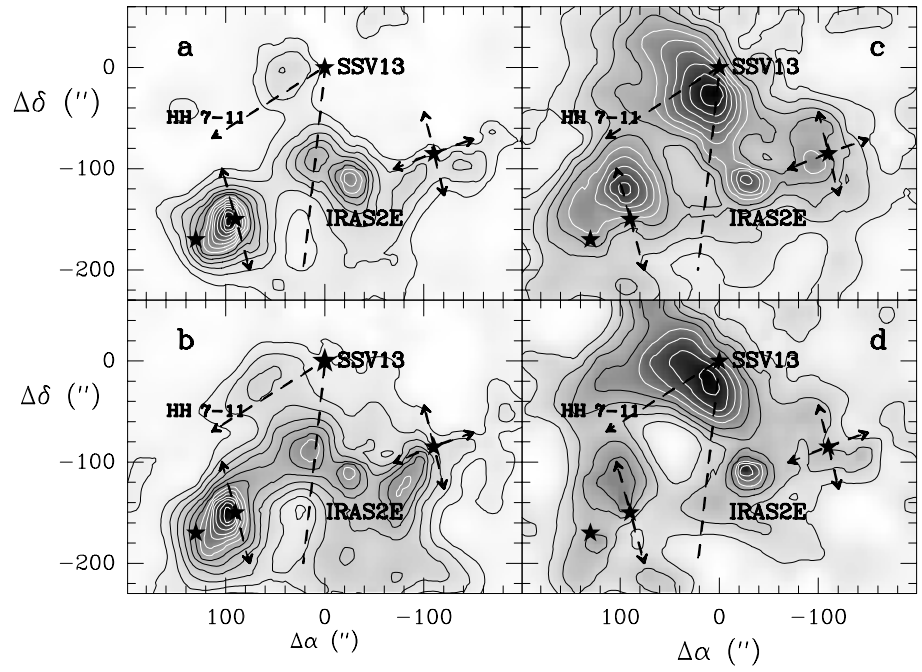


**Fig. 6a–d** Channel maps of the CS $J = 5 \rightarrow 4$ emission from the southern part of NGC1333. The panels **a-d** correspond to the 6.6, 7.2, 8.2 and 8.6 km s$^{-1}$ channel map respectively. Each channel map has a width of 0.2 km s$^{-1}$. Contour levels start from 0.25 K km s$^{-1}$ and increase in steps of 0.25 K km s$^{-1}$.

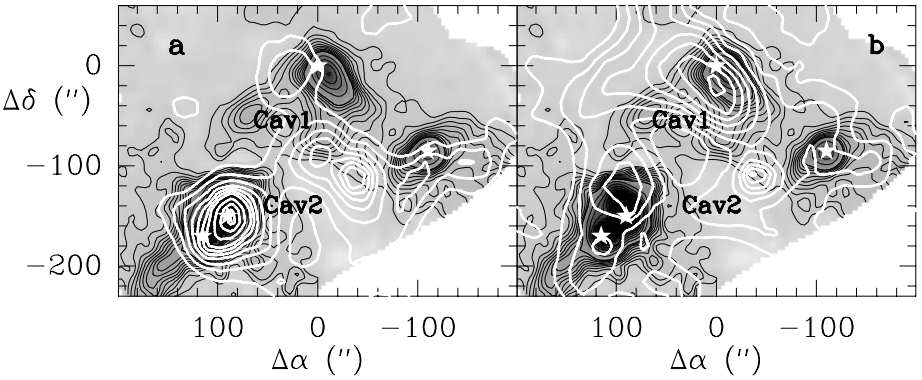


**Fig. 7a and b** Superimposition of the CS $J = 5 \rightarrow 4$ emission (white contours) at $v = 7.2$ km s$^{-1}$ (panel **a**) and $v = 8.6$ km s$^{-1}$ (panel **b**) upon the 1.25mm continuum emission (grayscale and dark contours). CS emission: first contour and contour interval are 0.25 K km s$^{-1}$. Continuum emission: contour levels range from 10 to 100 mJy beam$^{-1}$ by steps of 10 mJy beam$^{-1}$, then from 150 to 400 mJy beam$^{-1}$ by steps of 50 mJy beam$^{-1}$.

actually centered on a small CS clump, south of which appears the large clump observed by us. Whereas CS is detected along the HH 7-11 outflow, there is no counterpart in the opposite direction, North-West of SVS13. Inspection of individual velocity channel maps shows that at velocities $< 7.0$ km s$^{-1}$ the SVS13 CO high-velocity outflow and the associated $H_2$ jet are situated to the north of the CS bridge and propagate in a direction parallel to it. Close to its powering source, the jet advances between the bridge and a small condensation ($40''$ diameter) made of blueshifted gas (it is still detected at v= 6.4 km s$^{-1}$). At higher velocities ($v = 8.6$ km s$^{-1}$, Fig. 6d), an extension protruding from the northern part of the SVS13 core extends approximately parallel to the HH 7-11 outflow. Molecular observations of this outflow have shown that it is the blueshifted wing which propagates southeast of SVS13 into the molecular gas (Liseau et al. 1988; Bachiller & Cernicharo, 1990). Therefore, the redshifted component observed in CS $J = 5 \rightarrow 4$ does not trace material entrained by the flow.

### *4.2. Densities n($H_2$) and CS column densities*

In LCL we speculate that the outflows originating from the stars inside the pear-shaped cavity have compressed the surrounding shell of gas triggering the next generation of stars. To test this part of the scenario we checked the evolution of the density n($H_2$) and CS column density N(CS) in the compressed layer on the edge of the pear-shaped cavity. As we had no measurable CS $J = 5 \rightarrow 4$ at this location we used the $J = 2 \rightarrow 1$ and $J = 3 \rightarrow 2$ transitions. To perform these estimations the $J = 3 \rightarrow 2$ spectra have been degraded to the resolution of the $J = 2 \rightarrow 1$ ($27''$). The line parameters have been extracted following the method described in LCL. To derive n($H_2$) and N(CS) we used an LVG model with the Green & Chapmann (1978) CS collision rates. Consistent results were obtained with $T_k$ = 40 K (see LCL). We evaluate n($H_2$) and N(CS) along a constant declination line (dec = $96''$) which crosses the cavity borders. The results are presented in Fig. 8. The density increases when we cross the compressed layer while the column density decreases

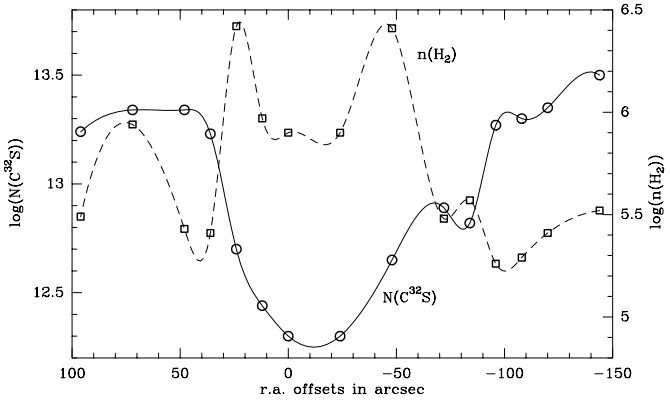


**Fig. 8.** Variation of log(n($H_2$)) and log(N(CS)) as a function of right ascension along the 96″ declination line. The $H_2$ density and CS column density have been evaluated from the CS $J = 3 \rightarrow 2$ and $J = 2 \rightarrow 1$ transitions with the use of an LVG model (see text).

in the center of the cavity. However due to observational uncertainties, i.e., beam dilution (the beam size at 90 GHz = 27″) and low signal to noise of the $J = 3 \rightarrow 2$ transition in the cavity, we should take these results with great care. Because we have no measurable CS $J = 5 \rightarrow 4$ measurements in this region, the thickness of the compressed layer around the shell should be much lower than 0.02 pc (= one telescope beam at this frequency). Furthermore, the gas structure around the cavity is rather complex, i.e. "gruyere-like" as discussed in Sect. 5.

### *4.3. CS abundances and masses from molecular measurements*

To estimate the fractional abundance of CS we determined the total $H_2$ column density using observations made with the 30m of the $C^{18}O$ $J = 2 \rightarrow 1$ transition. We made these observations in the East bow-shock of IRAS2 (IRAS2E) where the kinetic temperature is estimated to be about 40 K. As the $C^{18}O$ molecule traces all the gas in the line of sight, the gas density n($H_2$) was chosen to be equal to $5.0 \times 10^4$ cm$^{-3}$ a mean value which takes into account the density in the bow shock ($\simeq 10^6$ cm$^{-3}$; see Table 1 in LCL) and the lower density of the foreground and background ambient material ($\simeq 3 \times 10^3$ cm$^{-3}$). With these densities the $C^{18}O$ $J = 2 \rightarrow 1$ excitation temperature $T_{ex}$ is very close to the kinetic temperature $T_{kin}$. We estimated the $C^{18}O$ column density using an LVG model. In the 7 and 8 km s$^{-1}$ layers we obtain N($C^{18}O$) $\approx$ 7.8 $10^{14}$ cm$^{-2}$ and 2.5 $10^{15}$ cm$^{-2}$, respectively. We converted N($C^{18}O$) into N($H_2$) assuming N($H_2$) /N($C^{18}O$) $= 4 \times 10^6$ (Cernicharo & Guélin 1987). Using the CS column density determined at this location (Table 1 in LCL) we obtain X(CS) $\sim 1.2 \times 10^{-8}$ in the 7 km s$^{-1}$ layer and X(CS) $\sim 1.4 \times 10^{-9}$ in the 8 km s$^{-1}$ layer.

The uncertainties in the column density determinations are largely dominated by opacity effects rather than temperature variations (in Table 1 of LCL it is shown that N(CS) remain almost constant (within 10 %) when the kinetic temperature increases from 20 to 40 K). The impact of the CS lines opacity on the derivation of the physical parameters has been discussed in detail by González-Alfonso & Cernicharo (1993) (see their Appendix A). They conclude that the $J = 2 \rightarrow 1$ and $J = 3 \rightarrow 2$ lines will be affected by the surrounding envelope. Conversely the $J = 5 \rightarrow 4$ line opacity is negligible in the low-density gas and the photons emitted will escape the cloud.

As $C^{18}O$ is tracing a larger amount of material than CS, these CS abundances should be considered as lower limits. The deduced CS abundance in the 7 km s$^{-1}$ layer is likely due to the impact of the IRAS2 red outflow onto this layer (LCL) giving rise to a strong gas compression and a high CS fractional abundance (Sandell et al. (1994)). The X(CS) values derived by us are much lower than the high relative abundances obtained by Sandell et al. (1994)($1.4\,10^{-7}$). This is probably because these authors made use of a too low $T_{ex}$ temperature (see also LCL).

To derive the mass of the IRAS4 region, we adopted a CS fractional abundance of $2.0 \times 10^{-9}$. Then, if the IRAS4 surface is $50'' \times 70''$ we obtain a total mass of 4 $M_\odot$ in agreement with the mass determined from continuum observations. Using the same CS fractional abundance we also estimated the IRAS2 mass and obtained 1 $M_\odot$ a value much lower than the mass obtained from continuum observations (see above). However, in IRAS2 we have the case of a possible CS depletion on grains which will result in a lower fractional abundance and a higher mass. As a matter of fact the various positions observed in this cloud are probably chemically distinct from each other giving rise to different CS fractional abundances and making the determination of masses from CS observations rather uncertain. Better estimates should be obtained from $C^{18}O$ observations.

## 5. Discussion

In this section we bring together the CS and continuum observations to analyze the overall structure of the cloud, the formation of the cores, and the effect of star formation on the evolution of placentary material and the surrounding medium.

### *5.1. CS and continuum cores*

Among the three southern dust cores only IRAS4 shows a strong coincidence of the continuum and CS $J = 5 \rightarrow 4$ emissions (see e.g. Fig. 7). The CS maximum seen to the north of IRAS4 results from interaction of the north-south outflow driven by the IRAS4A source and the 8 km s$^{-1}$ layer. For the IRAS2 dust core there is no coincident CS core but only a weak elongated CS feature offset to the south-east by 15″(Fig. 7b). Similar displacement between the dust and gas emission are observed for SVS13 (see Fig. 7) and also IRAS7 and Cor1.

There are a number of possible explanations for the displacement in peak emission between the CS and continuum cores. The dust continuum emission is linearly proportional to dust column density times dust temperature whereas the CS $J = 5 \rightarrow 4$ emission may be strongly dependent on gas temperature and density : the J= 5 level lies about 24K above the ground state and its coefficient of spontaneous deexcitation is $\approx 3\,10^{-4}$ s$^{-1}$. Furthermore there is no assurance that the CS fractional abundance remains constant in a chemically active

region. Indeed depletion of CS onto grains is likely to be important at the high densities and low grain temperatures expected in the cold cores. Therefore it is not surprising to find a spatial displacement between the peaks in the dust continuum and the CS $J = 5 \rightarrow 4$ emission.

The situation appears more complicated for SVS13 as, in addition to a near-infrared Class I source, several other protostellar sources have been discovered in this core (Grossman et al. 1987, Rodríguez et al. 1997). All these sources contribute to heat the molecular gas and dust. One possible explanation for the lack of contrast in the CS emission is the dispersion of the very dense gas by the SVS13 outflows.

As noted in Sect. 3 the continuum map shows a number of peaks, most of which are associated with well known IR sources (see Fig. 1). However, one of these peaks, namely the weakest one (Cor1), is not associated with any known object. It is not associated with any strong CS peaks in either the CS $J = 5 \rightarrow 4$ or $J = 3 \rightarrow 2$ maps, although the CS $J = 5 \rightarrow 4$ has a local peak nearby. This continuum core may be in a pre-stellar stage. That is it is sufficiently evolved and dense that highly polar molecules such as CS have depleted onto grains, but not yet sufficiently dense at its center to form a protostar, or to have even started to collapse. In the northwest of the CS $J = 5 \rightarrow 4$ map there are two peaks associated with the SVS11 and SVS12 IR sources. Unfortunately, our continuum maps do not extend this far and we do not know if there are any coincident or nearby continuum cores. We speculate, however, based on the relationship between the CS $J = 5 \rightarrow 4$ and continuum peaks in the maps that continuum cores should be located nearby.

### *5.2. Comparison of gas and dust column densities*

A few positions were observed in $C^{18}O$ $J = 1 \rightarrow 0$ and $J = 2 \rightarrow 1$ around each dust core. We performed additional cuts along the IRAS2 and IRAS4 envelopes. From the densities estimated in NGC1333 (see Table 1), we conclude that the lower levels of $C^{18}O$ are very likely to be populated according to the LTE. We also assumed that the line opacities are low -we discuss this point below- and adopted the same kinetic temperature as for the dust to derive the $C^{18}O$ column densities at 3 and 1mm. To estimate the gas-to-dust ratio, we computed the ratio K of the $H_2$ column densities derived from $C^{18}O$ and dust emission respectively. In the case of the $C^{18}O$ $J = 1 \rightarrow 0$ transition, the dust emission was degraded to the same spatial resolution. The results obtained at 3mm in the protostellar sources are summarized in Table 1.

In the quiescent molecular gas (position of Cor1) and around IRAS7, the values of K are of a few (1.5 - 3). This ratio is found to be much lower at the positions of the other protostellar sources, especially the Class 0 sources : typically $\leq 0.1$ in IRAS2 and IRAS4A-B; it is higher in SVS13 : 0.3 - 0.5. Remarkably, K systematically increases in the envelope with farther distance to the protostar, to reach values of a few, close to those derived for the quiescent molecular gas. We examine below the effects which could account for such variations.

K is proportional to the product of dust and gas temperatures (at first order). However, as the dust temperatures are close to the gas kinetic temperatures for all protostars (see Sect. 3.4), it is unlikely that a thermal decoupling between both species be really efficient, at least to induce variations as large as those observed. Another uncertainty in the K determination result from a possible variation of $\kappa_\nu$ with burying of sources. As pointed out by Mezger et al. (1992), gas depletion onto grains around deeply embedded sources is not expected to change the dust absorption cross-section by more than a factor of 2. Therefore, unless the dust spectral index be noticeably modified in the central parts of very dense cores, the variations observed across the envelope and the central core of the protostars IRAS2 and IRAS4 are difficult to explain by changes in the dust emission properties.

On the other hand, we cannot exclude that the increase of the $C^{18}O$ lines opacity in the central parts of the protostellar cores results in a large underestimation of the gas column densities. However, we note that similar gas-to-dust variations are also observed in the envelopes of protostars, where the $C^{18}O$ lines are optically thin. *An underabundance of molecules in the cold dense protostellar cores by a factor of 5-10 as a result of depletion onto dust grains appears much more plausible to us.* Observations of a more optically thin tracer such as e.g. $C^{34}S$ are required to definitely ascertain this conclusion. In addition, observation of the dust emission at shorter wavelengths will be necessary to characterize the dust emission. In particular, the determination of the dust size distribution is a mandatory step in getting a better estimation of the column density of dust. Depletion of molecules in the collapse phase of molecular cores has been considered in the past as an explanation of the observed lack of contrast in the emission in and around protostellar cores (Mezger et al. 1988). Our observations, although seem to indicate that it is the case, can not rule out the possibility of opacities larger than 1 in the $C^{18}O$ lines. The available correlations between the column density derived using $C^{18}O$ and the visual extinction $A_v$ have been established for visual absorptions lower than 10 mag (Cernicharo and Guélin 1987). For a cloud with $A_v = 80$ mag, density $n(H_2) = 10^6$ cm$^{-3}$ and standard abundance $X(C^{18}O) = 2.5\,10^{-7}$, and excitation temperature $T_{ex} = 20K$, the expected opacity of the $J = 1 \rightarrow 0$ and $J = 2 \rightarrow 1$ lines of $C^{18}O$ are 1.1 and 3.1 respectively for typical linewidths of 1 km s$^{-1}$. However, for the same conditions, the dust opacity at millimeter wavelengths will be certainly $\ll 1$.

### *5.3. Cavities, $H_2$ jets and molecular outflows*

The millimeter continuum and CS line observations have shown the presence of two "holes" of emission (Cav1 and Cav2) in the vicinity of SVS13 and IRAS4 (see e.g. Fig. 7). As these holes are detected in different velocity ranges, we conclude that it is not an artifact resulting from the presence of matter on the line of sight (making two cavities appear from a single one) but instead that Cav1 and Cav2 are two distinct entities. We now assess the possibility that these cavities have been dug by the jets powered by the surrounding protostellar sources.

Cav1 is bounded to the West by the southern extension protruding from the SVS13 dust core and to the North by the arc of dust and gas extending from SVS13 parallel to the HH 7-11 molecular outflow. Comparison with $H_2$ emission shows that some filamentary structures reported by HL95 spatially coincide with the interface between the cavity and molecular gas (Fig. 1 and Fig. 4). Dense gas around the cavity (as traced by CS) appears redshifted with respect to the ambient gas layers by $0.5 - 1$ km s$^{-1}$ south of SVS13, but the (blueshifted) counterpart if also detected close to the exciting source (Fig. 6). We are therefore observing a cavity (whose walls are detected in $H_2$) surrounded by dense compressed gas expanding in the ambient medium. Taking into account the close association between the dense gas around the cavity and the powering source of the energetic flow HH 7-11, it seems likely that Cav1 was dug by the latter during the course of its propagation in the molecular gas.

Our study shows the same physical properties for Cav2 as for Cav1, which suggests a similar origin to Cav2. However, there is no signature of molecular outflows associated with the cavity. We speculate that Cav2 could have been evacuated earlier by an outflow either no longer present or too weak to be detected. Due to the location of the cavity, IRAS4 would probably be the powering source of the outflow, if any, propagating East-West. This might seem contradictory with the direction of the IRAS4A outflow observed by (Sandell et al. 1994) which makes a projected angle of 45° with respect to the North. However, a) the present flow originates from IRAS4A which is known to be a protostellar cluster, as well as IRAS4B (Lay et al. 1995); b) there is increasing evidence for a precession between successive outflow events at even very large angles (Eislöffel et al. 1996, Ladd & Hodapp 1997). Inspection of the $H_2$ map of HL95 reveals a faint isolated component *inside Cav2*, strongly resembling the *bow-shock of a jet moving towards West* at $\alpha \approx 03^h25^m54^s$, $\delta \approx 31°03'30''$ (its position is indicated by a black square on Fig. 1). Tracing back the trajectory of the jet leads to IRAS4B. As IRAS4B is the only protostellar source aligned with the jet, we conclude it is probably its driving source. The weakness of the emission suggests that the ejection is already ancient, which agrees with the idea of a low-density, now evacuated, cavity.

### *5.4. Dynamics of the growth of cavities*

Our continuum and molecular observations give new insight about how the molecular outflows emanating from the young stellar objects shape the molecular clouds and ignite the next generation of star formation. It is now well accepted that each young stellar object undergoes in its life violent outflows which tend to dissipate their surrounding cocoon. These outflows dig cavities with various geometries and volumes depending on the energy in the flows and the density and pressure of the surrounding material. Such a scenario had already been proposed to account for the molecular gas dynamics around the HH1-2 and HH34 nebulae (Martin-Pintado & Cernicharo, 1987; Cernicharo 1991). Our observations clearly confirm this model and show that cavities can be evacuated very efficiently already in the early stages of protostellar evolution. In addition, such cavities from nearby young stellar objects expand to eventually overlap and form larger cavities. The SVS13 southern gas extension gives hint of such a process. We first note that the morphological appearance of the neighboring $H_2$ structure ASR20-21 suggests it traces more probably the wall of a cavity than a jet. Hence, the dust and molecular emission extending south of SVS13 are comprised between the walls of two cavities distant from each other by $\approx 0.025$ pc. Indeed the large pear-shaped cavity discovered by WCLWP and LCL probably formed this way.

WCLWP proposed that the star formation in NGC1333 was the result of sequential star formation initiated by SVS13. The outflow from this source would have created a cavity and compressed the surrounding material initiating the second stage of star formation in the compressed shell. The second generation would have swept up more material creating a larger cavity and compressing the gas further. The first consequence of this scenario is an isotropic increase of the density in the surrounding shell together with an isotropic ignition of a new generation of stars. Obviously, even if we observe more star formation in the surrounding shell than in the rest of the cloud, the distribution of new born stars is not limited to the edge of the cavity.

The results presented in this paper modify this scenario. First, as pointed out in LCL, SVS13 is probably not the only initiator of the NGC1333 star formation but rather one of them. Second, the increase in density is more distributed in the cloud, depending on the size and shape of the cavity dug by the outflows emanating from the new born stars. The presence of many YSO objects in the pear-shaped cavity (see Fig. 1 of LCL) is certainly responsible for the creation of this large cavity and for the numerous stars formed in the surroundings. However, there exist other new born stars in the cloud which certainly result from a nearby older star formation.

## 6. Summary

We have mapped the NGC1333 star formation region in the continuum and molecular CS $J = 5 \rightarrow 4$ emission. The described observations allowed us to determine the physical properties of the dust and gas, and to derive relationships between the cloud and the embedded stellar objects. The main results can be summarized as follows:

1. In addition to the conspicuous dust envelopes and cores associated with protostars IRAS4A-B, IRAS2 and SVS13, we have detected two fainter dust condensations corresponding with IRAS7 and one starless core. With the exception of IRAS4 and IRAS7 all these condensations are located near the edge of a large cavity void of any emission, which coincides with the cavity already identified by WCLWP and LCL from $C^{18}O$ and CS molecular observations. The CS $J = 5 \rightarrow 4$ emission which traces the dense and warm gas is observed in all the dust cores. However only IRAS4 shows a strong spatial coincidence of the continuum and CS $J = 5 \rightarrow 4$ emission. In all other cores the CS molecular emission appears offset from the continuum peak.
2. Our continuum map reveals also the presence of material associated with the protostars outflow(s). The large-scale

continuum emission mostly traces dense material around two additional small cavities void of dust and CS molecular emission. The first one (Cav1) is opened to the southeast of SVS13 and is situated between the HH 7-11 chain of objects and the SVS13 southern elongation. The second one (Cav2) is delimited by an arc of gas which connects IRAS4 to the southern SVS13 extension and IRAS2E. Their edges are detected in the $H_2$ S(1) v=1-0 line. The CS $J = 5 \rightarrow 4$ traces dense blue/redshifted gas around these cavities, suggesting they are expanding into the circumstellar medium with velocities of $0.5 - 1$ km s$^{-1}$. Comparison of dust and molecular emission suggests that Cav1 has been excavated by the HH 7-11 outflow, powered by SVS13, and that Cav2 would have been dug by an outflow originating from IRAS4B, now too weak to be detected.

3. Comparison of the column densities derived from $C^{18}O$ and dust observations shows that the gas-to-dust ratio systematically increases with farther distance to the protostars. This suggests that molecules are depleted onto grains in the cold dense protostellar cores, although large opacities effects in the $C^{18}O$ lines resulting in large underestimations of the gas column densities cannot be excluded.
4. These continuum and molecular observations give rise to a modified NGC1333 sequential star formation scenario. First SVS13 is probably not the only initiator of star formation in NGC1333 but rather one of them. Second our observations have shown that the outflows dig cavities with various geometries and volumes and could be responsible for the next generation of star formation in their vicinity. The presence of many YSO objects in the pear-shaped cavity (LCL) has been responsible for the creation and enlargement of this large cavity and for the numerous young stellar objects formed in the edge. However there exist others YSOs outside this huge cavity which result from nearby star formation. Then, instead of the "centrally sequential" star formation process proposed by WCLWP, this might favor a "distributed sequential" star formation scenario in NGC1333.

*Acknowledgements.* We thank Dr. S. Cabrit for her critical comments on an earlier version of the manuscript. JC thanks the Spanish DGES for support through grant ACP96-0168 & ESP96-2529-E. The research of WL was undertaken at the Jet Propulsion Laboratory, California Institute of Technology under support by the National Aeronautics and Space Administration.

## References

Aspin, C., Sandell, G., Russel, A.P.G. 1994, A&AS, 106, 165
Aspin, C., Sandell, G. 1997, MNRAS, to be published
Bachiller, R., Cernicharo, J. 1990, A&A, 239, 276
Blake, G.A., Sutton, E.C., Masson, R.C., Phillips T.G. 1987, ApJ, 315, 621
Blake, G.A., Sandell, G., Van Dishoeck, E.F., Groesbeck, T.D., Mundy, L.G., Aspin, C., 1995, ApJ, 441, 689
Cernicharo, J., Bachiller, R., Duvert, G., 1985, 149, 273
Cernicharo, J., Guelin, M., 1987, A&A, 176, 299
Cernicharo, J., 1991, "The Physics of Star Formation and Early Stellar Evolution", p. 287, Ed. C. Lada & N. Kylafis, NATO ASI Series, Kluwer Academic Press.
Dent, W.R.F., Cunningham, C., Hayward, R., Davies, S.R., Wade, D., Avery, L.W., Mayer, C.J., Masuda, N.T. 1993, MNRAS, 262, L13
Draine, B.T., & Lee, H.M., 1984, ApJ, 285, 89
Eislöffel, J., Smith, M.D., Davis, C.J., Ray, T.P. 1996, AJ, 112, 2086
González-Alfonso, E., Cernicharo, J., 1993, A&A, 279, 506
Green, S., Chapman, S. 1978, ApJS, 37, 169
Grossman, E. N., Masson, C. R. Sargent, A. I., Scoville, N. Z., Scott, S., Woody, D. P. 1987, ApJ, 320, 356
Gueth, F., Guilloteau, S., Bachiller, R. 1996, 307, 891
Hodapp, K.-W., & Ladd, E.F. 1995, ApJ, 453, 715, (HL95)
Jennings, R.E., Cameron, D.M.H., Cuddle, W., Hirsute, C.J. 1987, MNRAS, 226, 461
Ladd, E.F., Hodapp, K.-W. 1997, ApJ, 474, 749
Lada, C.J., Alves, J., Lada, E.A., 1997, AJ, 111, 1964
Langer, W.D., Castets A., Lefloch, B. 1996, ApJ, 471, L111 (LCL)
Lay, O.P., Carlstrom, J.E., Hills, R.E. 1995, ApJ, 452, L73
Lefloch, B., Castets, A., Langer, W.D. 1997, in prep
Liseau, R., Sandell, G., Knee, L.B.G. 1988, A&A, 192, 153
Martin-Pintado, J., Cernicharo, J., 1987, A&A, 176, L27
Mehringer, D.M. 1996, ApJ, 462, 355
Mezger, P.G., Chini, R., Kreysa, E., Wink, J.E., and Salter, C.J. 1988, A&A, 191, 44
Mezger, P.G., Wink, J.E., Zylka, R. 1990, A&A, 228, 95
Mezger, P.G., Sievers, A., Zylka, R., Haslam, C.G.T., Kreysa, E., Lemke, R. 1992, A&A, 265, 743
Rodríguez, L.F., Anglada, G., Curiel, S. 1997, ApJ, 480, L125
Rudolph, A.L., Bachiller, R., Rieu, N.-Q., Trung, D.V., Palmer, P., Welch, W.J., 1997, ApJ, submitted
Sandell, G., Aspin, C., Duncan, W.D., Robson, E.I., Dent, W.R.F. 1990, A&A, 232, 347
Sandell, G., Aspin, C., Duncan, W.D., Russel, A.P., Robson, E.I. 1991, ApJ, 376, L17
Sandell, G., Knee, L.B.G., Aspin, C., Robson, E.I., & Russel, A.P.G. 1994, A&A, 285, L1
Strom, S.E., Vrba, F.J., Strom, K.M., 1976, A.J., 81, 314
Swade, D.A. 1989, ApJ, 345, 828
Warin, S., Castets, A., Langer, W.D., Wilson, R.W., & Pagani, L. 1996, A&A 306, 935 (WCLWP)
Ward-Thompson, D., Buckley, H.D., Greaves, J.S., Holland, W.S., André, P. 1997, MNRAS, 281, 53